Received: 10 August 2021 | Revised: 16 November 2021 | Accepted: 9 December 2021

DOI: 10.1002/jbt.22972

RESEARCH ARTICLE

WILEY

Selenium and silver nanoparticles: A new approach for treatment of bacterial and viral hepatic infections via modulating oxidative stress and DNA fragmentation

Sameh S. Gad[1] | Dina S. Abdelrahim[2] | Sameh H. Ismail[3] | Sherine M. Ibrahim[4]

[1]Department of Pharmacology, Faculty of Pharmacy, October University for Modern Sciences and Arts (MSA), Giza, Egypt

[2]Lecturer of clinical pharmacology, Faculty of medicine, Ain-Shams university, Cairo, Egypt

[3]Department of Pharmacology, Faculty of Nanotechnology for postgraduate studies, Cairo University, Sheikh Zayed Branch Campus, Sheikh Zayed City, Egypt

[4]Biochemistry Department, Faculty of Pharmacy, October University for Modern Sciences and Arts (MSA), Giza, Egypt

Correspondence

Sherine M. Ibrahim, Biochemistry Department, Faculty of Pharmacy, October University for Modern Sciences and Arts (MSA), Giza, Egypt.
Email: sherinemahmoud@msa.edu.eg

Abstract

Nanoparticles are recently playing a potential role in improving drug uptake and the treatment of diseases. A variety of nanoparticles, such as selenium nanoparticles (SeNPs) and silver nanoparticles (AgNPs) have been used as drug carriers in various ways for treatment of cancers and liver diseases. Our aim in this study is to investigate the ability of AgNPs and SeNPs to target and treat the viral and bacterial infection of the liver in rats and cell lines. For assessment of antioxidant activity of AgNPs in rats with induced liver bacterial infection, six adult male albino rats were included in this study, liver slices were taken and assigned to 6 groups. Markers of hepatic functions, oxidative stress, and inflammation in liver slices are carried out. Although for assessment of antiviral activity of SeNPs, hepatitis B virus transfected (HBV)-replicating human cell line HepG2 and normal hepatocyte cells were used, hepatic and inflammatory alterations are determined through quantitative polymerase chain reaction and comet assay techniques. The effect of AgNPs on interleukin-6 and tumor necrosis factor levels were reduced in different treated groups with AgNPs compared with the control and diseased groups. On the other hand, SeNPs revealed significant alterations in the inflammatory markers as well as DNA damage in the treated HBV-human cell line HepG2 compared to the diseased ones. AgNPs have the ability for producing various hepatic alterations and can inhibit the proliferation of hepatic stellate cells (HSCs) in a dose and size-dependent manner. On the other hand, SeNPs showed excellent selectivity towards viral cells in the HepG2 cell lines. Both AgNPs and SeNPs might be promising drug designs for treating viral and bacterial liver diseases.

KEYWORDS

interleukin-6, hepatitis B virus, oxidative stress, selenium nanoparticles, silver nanoparticles, tumor necrosis factor-α

Abbreviations: AFM, atomic force microscope; AgL, large silver nanoparticles; AgNPs, sliver nanoparticles; AgS, small silver nanoparticles; ALT, alanine transaminase; AST, aspartate transaminase; BET, Brunner-Emmett-Teller method; DAB, 3,3'-Diaminobenzidine; ELISA, enzyme-linked immunosorbent assay; GSH, glutathione; HBV, hepatitis B virus; HSCs, hepatic stellate cells; H&E, hematoxylin and eosin; IL-6, interleukin-6; IL-8, interleukin-8; LPS, lipopolysaccharide; MDA, malondialdehyde; NAC, *N*-acetyl cysteine; NOS, nitric oxide reactive species; PBS, phosphate buffer saline; PCR, polymerase chain reaction; ROS, reactive oxygen species; SEM, scanning electron microscope; SeNPs, selenium nanoparticles; TBARS, thiobarbituric acid reactive substances; TEM, transmission electron microscope; TGF, tumor growth factor; TNF-α, tumor necrosis factor; TSC, trisodium citrate; XRD, X-ray diffraction.

1 | INTRODUCTION

Nanoparticles have been widely investigated over the past decades, due to their special physical and chemical properties. The main properties of nanomaterials depend mainly on their morphology and particle size. Silver nanoparticles (AgNPs) and selenium nanoparticles (SeNPs) are the most commercialized nanoparticles used in medical research for medical applications such as gene, antimicrobial agents, and drug delivery carriers.[1]

AgNPs have been shown to significantly cure chronic liver diseases.[2] Additionally, these AgNPs have been used to target specific injured tissues in blood circulation through the combination of antibody-based targeting of ligands and material composition. Ag ions in sufficient concentration readily kill bacteria in vitro. These studies showed the potential effect of AgNPs for the cure of liver diseases including bacterial infection and hepatic fibrosis.[3]

Recently, traditional chemotherapy and anti-fibrotic treatments became ineffective in treatment of chronic liver diseases, due to the development of resistant drug tolerance. Thus, AgNPs may provide a safer therapeutic tool of treatment for targeting the hepatic stellate cells (HSCs), which are the main focus for treatment of liver cirrhosis and hepatic fibrosis.[4]

SeNPs are regarded recently as new nanoparticles and have attracted great interest due to their higher anti-inflammatory, antiviral and antitumor activity, lower toxicity to normal cells compared with other used nanoparticles.[5] Taken into consideration, selenium (Se) is an essential element that has many important functions in the human body including protection of the cardiovascular and liver organs, regulation of secretion of hormones, and free radical scavenger. Recent studies have shown that SeNPs have potential therapeutic action for treatment of many diseases including inflammation, virus infection, and cancer.[6] This new nanoparticle provides a promising tool for the treatment of many liver diseases.[7]

In this study, we will investigate the efficiency of AgNPs in treatment of liver bacterial infection in rats and the efficiency of SeNPs for targeting and treatment of HBV infected cell lines by evaluating their hepatic and inflammatory changes.

2 | MATERIALS AND METHODS

2.1 | Animal experimentation (bacterial infection and use of AgNPs)

2.1.1 | Preparation and synthesis of AgNPs

Two sizes of AgNPs were purchased from (Egypt Center for Nanotechnology), as small particle size (10 and 75 nm) and large particle size (250–300 nm). The size, morphology, and dispersion of the nanoparticles were characterized using a Tecnai™ G2 Twin Transmission Electron Microscope (FEI; Hillsboro) and dynamic light scattering (Compact Goniometer System 3; ALV-GmbH). Synthesis of AgNPs was achieved by precipitation method using trisodium citrate (TSC) as reducing agent and capping one at the same time. $AgNO_3$ solution (0.03 M) was dissolved in 200 ml deionized water, heated to boiling, then 0.3 M TSC was added drop by drop with slowly stirring and heat until the color of the solution become pale yellow. The final solution was cooled at room temperature in an isolated dark area to avoid light.[8]

2.1.2 | Animal experimentation (bacterial infection)

Six adult male albino rats weighing from 200 to 250 g were used. Rats were housed at MSA animal house under standard laboratory conditions and suitable temperatures. They were housed in plastic cages, given a standard normal diet and water. The work was done according to ethical committee guidelines in the faculty of pharmacy and animal experimentations guideline at MSA University (**code: PH8/EC8/2019F**). After reaching to target weight (250 g), animals were sacrificed to take their livers.

The livers were immediately frozen then kept in the fridge for 24 h. Then, precision-cut liver slices were carried out using a Cryostat microtome device in Animal health research institute, the thickness of the slice was optimized to 150 μm. The freshly liver slices (14 slices each 150 μm thickness) are transferred to a six-well plate under controlled physiological conditions. We used a six-well plate and distribute the slices evenly, every well contained two slices exactly. So, all the wells contain the same weight and characterization. The six-well plate was assigned as follows; group 1: (Normal) containing Ringer solution only. Group 2: (control) lipopolysaccharide (LPS) used for induction of bacterial infection in rats 0.5 ml of (5 mg/13 ml distilled water) + Ringer solution, Group 3: (standard treatment) LPS 0.5 ml of (5 mg/13 ml distilled water) + 0.5 ml N-acetyl cysteine (NAC) used as standard treatment for bacterial infection 50% solution + Ringer solution, Group 4: (treatment II) LPS 0.5 ml of (5 mg/13 ml distilled water) + small sliver nanoparticles (AgNpS) 0.5 ml 50% solution (1–100 nm) + Ringer solution, Group 5: (treatment III) LPS 0.5 ml of (5 mg/13 ml distilled water) + large sliver nanoparticles (AgNpL) 0.5 ml 50% solution (150–300 nm) + 2 ml Ringer solution, Group 6: LPS 0.5 ml of (5 mg/13 ml distilled water) + 0.5 ml 50% solution NAC + AgNpS (1–100 nm) 0.5 ml 50% solution + 2 ml Ringer solution, and Group 7: LPS 0.5 ml of (5 mg/13 ml distilled water) + 0.5 ml NAC 50% solution + AgNpL (150–300 nm) 0.5 ml 50% solution + 2 ml Ringer solution.

In all wells the ringer solution was added equally; The plates were then incubated in a humidified incubator in the research lab at MSA University under conditions of 95% oxygen and 5% carbon dioxide to maintain slices viability. After 24-h incubation, plates were gently removed and the supernatant and tissue homogenate were all collected and then subjected for analysis. The same steps were repeated six times with each rat $n = 6$.

2.1.3 | Hepatic function tests analysis

Serum aspartate aminotransferase (AST) and alanine aminotransferase (ALT) were assayed in liver slices using (Biodiagnostics).

2.1.4 | Oxidative stress analysis

GSH assay: Liver slices were kept frozen at −20°C and tissue homogenate was made in a glass homogenizer using 5% 5-suphosalicylic acid for (GSH). GSH level was assayed using the dithio-binitrobenzoic acid method.[9]

2.1.5 | Cytokine detection

The quantity of anti-inflammatory markers; interleukin 6 (IL-6) and tumor necrosis factor-α (TNF-α), in the liver slices homogenate-conditioned medium was quantified using an enzyme-linked immunosorbent assay (ELISA) kit (MyBiosource, Inc.) according to the manufacturer's instructions.

2.1.6 | Histopathological and immunohistochemistry assessment

After fixation of liver specimens in 10% formaldehyde in phosphate-buffered saline (PBS), liver slices were then dehydrated, embedded into paraffin, and sections were made at a thickness of 5 µm. These sections were carefully stained with hematoxylin and eosin (H&E) for histopathology.[10] Briefly, liver tissue sections were cut into 5 µm sections and subjected to deparaffinization and heat-induced antigen then endogenous peroxidase and protein blocking steps. After washing, liver tissue sections were incubated with primary antibodies (anti-CD68; Santa Cruz Biotechnology Inc.) overnight at 4°C with a dilution ratio of 1:200 in PBS. HRP-labelled secondary antibodies (Abcam) were applied for 2 h after washing. Finally, the DAB-substrate kit was then used for color development and Meyers hematoxylin was used as counterstain.

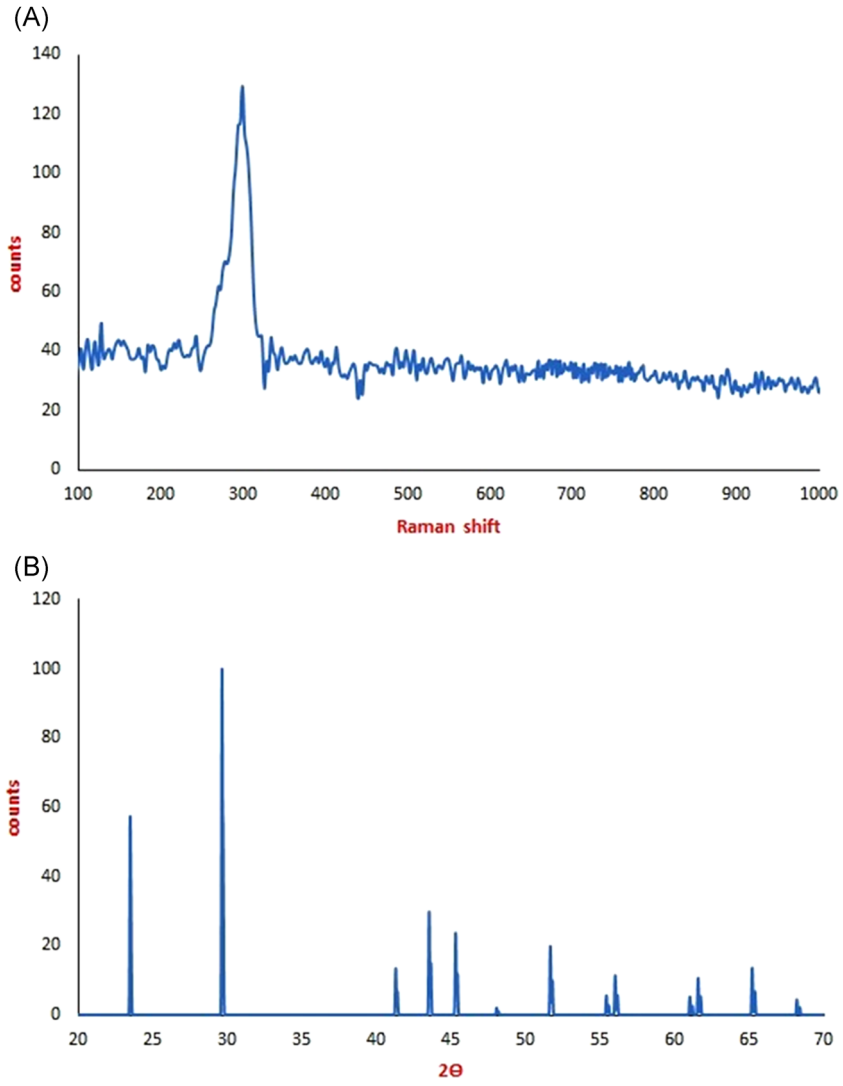

FIGURE 1 (A) Raman spectrum of colloidal SeNPs showing no contaminated peaks with a very strong sharp peak at 300 cm^{-1} and (B) X-ray Diffraction (XRD) pattern of SeNPs showed the characteristic peaks for SeNPs at 2θ, 23.5°, 29.6°, 41.3°, 43.5°, 45.3°, 48.2°, 51.7°, 56°, 56.1°, 61°, 61.2°, 65.2°, 68.2°, and 68.4°

2.2 | Cell culture (viral infection and use of SeNPs)

2.2.1 | Preparation of SeNPs

Synthesis of SeNPs has been done by precipitation—sonochemical method using ascorbic acid and TSC as a reducing-capping agent at the same time. Na_2SeO_3 solution (0.1 M) was dissolved in 120 ml of doubled deionized water until the solution become colorless using ultrasound instrument Hielscher 400UP_S, Germany at an amplitude of 74% for 1 min at a temperature of 45°C. Then a mixture of ascorbic acid and TSC (0.2–0.1 M for ascorbic acid and TSC, respectively) is added drop by drop until the color of the mixture becomes pale brown. The solution was cooled at room temperature in the dark condition.[11]

2.2.2 | Cell culture (viral infection)

HBV-transfected replicating human HCC cell line HepG2 and normal hepatocyte cells were purchased from Guangzhou Jennio Biotech Co., Ltd. Cell lines were maintained in Dulbecco's modified Eagle's medium supplemented with 10% fetal bovine serum. Cell lines were cultured at 37°C in a humidified chamber supplemented with 5% CO2. Group 1: normal hepatocyte cells served as the control group. Group 2: HBV-transfected replicating human HCC cell line HepG2 and Group 3: HBV-transfected-replicating human HCC cell line HepG2 treated with SeNPs.

Cells were incubated with HBV-positive sera (10^9 particles/ml) for 14 h at 37°C, washed extensively with PBS and a fresh medium was added. For polymerase chain reaction (PCR) analysis, at 4 days post-infection cells were washed extensively in PBS, collected using a rubber policeman, and lysed in a proteinase K lysis buffer for 6 h at 37°C, extracted with phenol-chloroform and precipitated with ethanol. The amount of DNA was determined by conducting semi-quantitative PCR analysis of HBsAg using (Brilliant II-PCR Master Mix Kit, 1-Step; Agilent).

2.2.3 | Determination of hepatic function tests and oxidative stress marker

The cell culture media from each of the 25 cm^2 culture flasks was collected, centrifuged at 3000*g* for 10 min, and stored at −70°C until assay. ALT and AST were assayed using (Biodiagnostics) while MDA

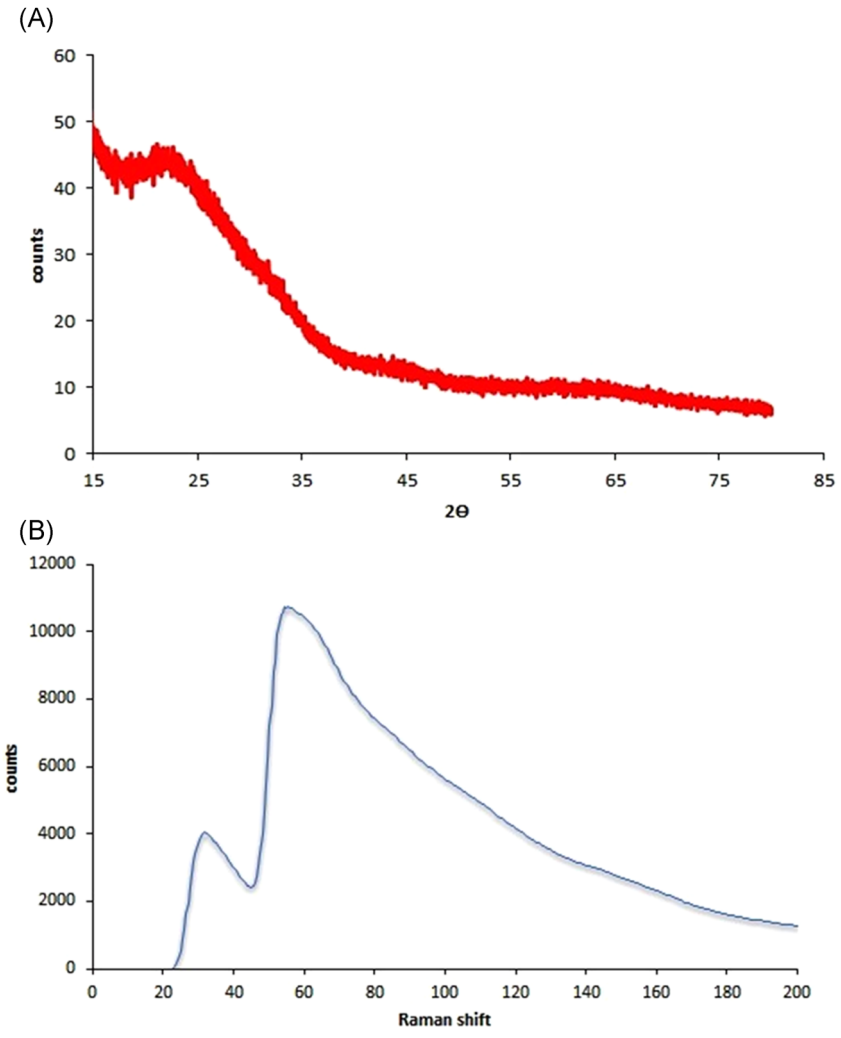

FIGURE 2 (A) X-ray diffraction (XRD) pattern of silver nanoparticles (AgNPs) illustrated the amorphous nature of AgNPs. (B) Raman spectra of amorphous AgNPs showed characteristic peaks at 52.1 and 146.5

was determined by the thiobarbituric acid reactive substances (TBARS) method.[12]

2.2.4 | Cytokine detection

IL-2 was determined using IL-2 ELISA Kit (ab46032) and IL-8 was measured using IL-8 (CXCL8) ELISA Kit for cell culture supernatants by following the kit protocol while TNF-α was assayed by following the ELISA kit protocol (Cat: KIT10602) and TGF was measured using TGF-α Human (ab100647).

2.2.5 | Quantification of HBV genomic DNA by real-time PCR

HBV genomic DNA extraction and sequencing analyses. HBV genomic DNA was extracted from the supernatants of cocultured HepG2 cells using a Viral DNA Isolation Kit (Qiagen) following the manufacturer's instructions. Briefly, cell supernatants were added to the virus lysis buffer, and the lysates were loaded onto the spin column. After viral DNA was bound to the membrane, the column was washed and finally, the viral DNA was eluted. PCR was performed using HBV genomic DNA as a template to amplify the X gene primer and probe sequences are as follows: forward primer HBV-F3, 5′-GGCCATCAGCGCATGC-3′, and reverse primer HBV-R3M3, 5′-C [5-NitIdI] GCTGCGAGCAAAACA-3′; and probe HBV-P3, 5′-R-CTCTGCCGATCCATACTGCGGAACTC-Q-3. The PCR conditions were: initial denaturation at 94°C for 2 min, followed by 35 cycles of 94°C for 30 s, 55°C for 30 s, and 72°C for 1 min, and a final extension was performed at 72°C for 10 min.

2.2.6 | Comet assay

The extent of DNA damage was accessed using the comet assay under alkaline conditions. Comet tail length was measured by fluorescence microscopy and then analyzed using CaspLab Comet Assay Software v1.2.3 (Tritek Corporation).

2.3 | Characterization of AgNPS and SeNPs

2.3.1 | Identification class

X-ray diffraction (XRD) Bruker D8 Discover device was used for XRD measurements. The X-ray source used was Cu Kα radiation with a current of 32 mA and voltage of 41 kV. The 2θ angles ranged from 20

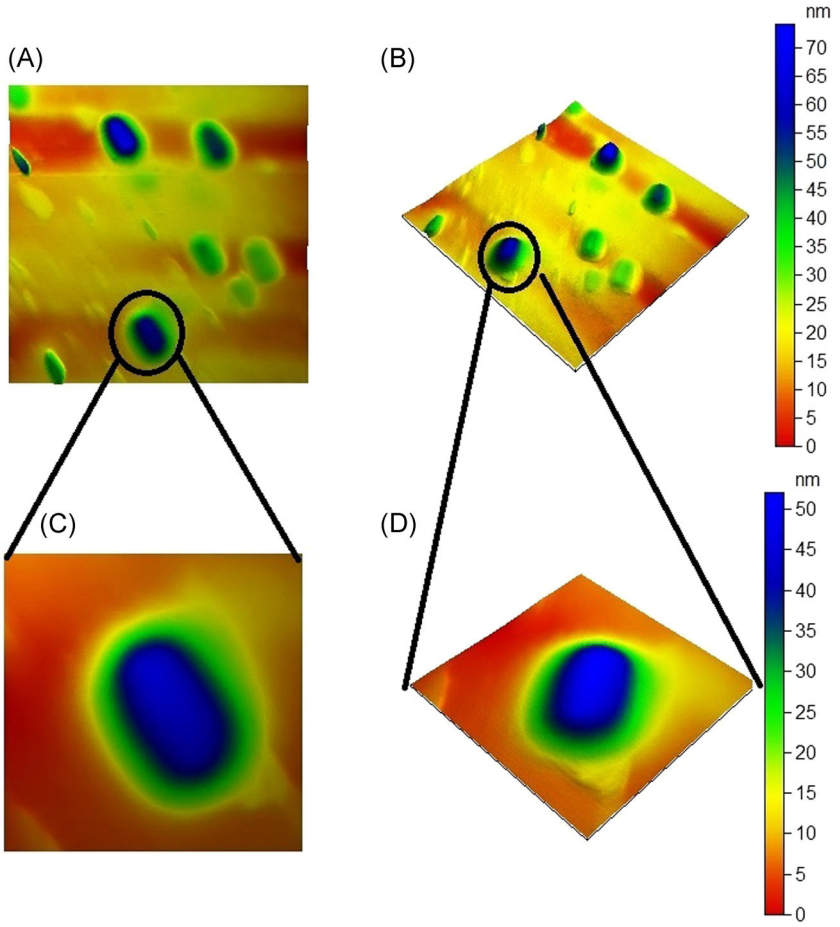

FIGURE 3 Atomic force microscope (AFM) image of colloidal selenium nanoparticles (SeNPs) nanoparticles. (A) Two-dimensional (2D) view AFM image of 200 nm × 200 nm size. (B) Three-dimensional (3D) view AFM image of 200 nm × 200 nm size. (C) 2D view AFM image of 100 nm × 100 nm size. (D) 3D view AFM image of 100 nm × 100 nm size. 2D and 3D AFM images and data showed that colloidal SeNPs nanoparticles samples have excellent homogenous surface topography. In addition, AFM images illustrated the rode shape (blue) with excellent caping of citrate (green) composed of core-shell nanostructure with a dramatic shape

to 70° for SeNPs and from 35 to 90° for AgNPs with a scan speed of 0.3°/min. The Raman spectra were achieved by a Horiba lab RAM HR evolution spectrometer. The 532 nm edge laser line with Raman shift range from 100 to 1000 cm^{-1} for SeNPs and AgNPs range from 20 to 200 cm^{-1}, grating (450–850 nm) and ND filter 10% to prevent oxidation of SeNPs and AgNPs. Acquisition time was 15 s, accumulations of 4 without spike filter and objective was ×100.

2.3.2 | Index class

BET method (the Brunauer–Emmett–Teller isotherm) was used to determine the specific surface area by pore and surface area analyzer manufacturer by Quantachrome, model of NOVA touch LX2. The sample was degassed at 80°C for 3 h. under vacuum. DLS and zeta potential are achieved by DLS and zeta potential analyzer (Malvern).

2.3.3 | Microscopic class

Atomic force microscope (AFM) (5600LS; Agilent) was used its 2D and 3D AFM images to determine the surface topography of SeNPs and AgNPs. First, samples were prepared by subjecting samples to ultrasound waves for 15 min, a condition of 50 kHz, at an amplitude of 44% and 0.45 of a cycle (Up 400 s manufacture by Hielscher, German). Finally, created a thin film using Spain coater instrument model Laurell-650Sz at the condition of 700 rpm under vacuum. AFM images and data profile have been done for 200 nm × 200 nm and its zoom 100 nm × 100 nm using contact mode, Al tap, 0.71 In/S speed, I. gain 2 and P. gain 4. Scanning electron microscopy (SEM) instruments have been used to study SeNPs surface morphology. The SEM images were achieved by Jol 2000, Japan. Transmission electron microscopy (TEM) study was performed by adding SeNPs to deionized water and sonicating for 15 min using ultrasound prop with a 60 kHz, at an amplitude of 41% and 0.41 of a cycle (Up 400 s; Hielscher). TEM experiments were achieved using (Jeol, JEM-2100 high-resolution).

2.4 | Statistical analysis

All data are expressed as mean ± SD. The difference between groups was statistically analyzed by GraphPad Prism 6, using one-way analysis of variance followed by Tukey's Kramer Multiple Comparison Test. $p < 0.05$ was considered as significant.

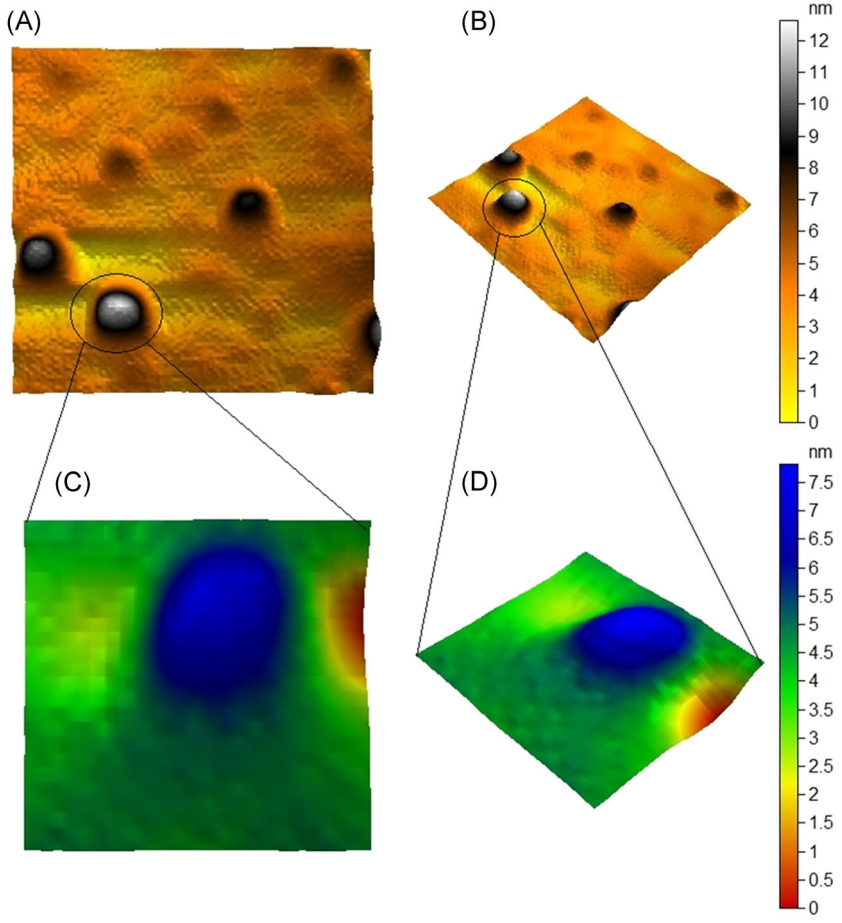

FIGURE 4 Atomic force microscope (AFM) image of colloidal silver nanoparticles. (A) 2D view AFM image of 200 nm × 200 nm size. (B) 3D view AFM image of 200 nm × 200 nm size. (C) 2D view AFM image of 100 nm × 100 nm size. (D) 3D view AFM image of 100 nm × 100 nm size. AFM images showed its spherical shape with very sharp edges and homogenous in size and shape. 2D, two-dimensional; 3D, three-dimensional

3 | RESULTS

3.1 | Characterization of AgNPs and SeNPs

3.1.1 | Identification

XRD pattern of SeNPs showed the characteristic peaks for SeNPs at $2\theta = 23.5°$, 29.6°, 41.3°, 43.5°, 45.3°, 48.2°, 51.7°, 56°, 56.1°, 61°, 61.2°, 65.2°, 68.2°, and 68.4° which as shown in Figure 1B). while the XRD pattern of AgNPs illustrated the amorphous nature of AgNPs as shown in Figure 2A. These results indicate the high crystallinity of SeNPs. Concerning the Raman spectrum of colloidal SeNPs, the characteristic Raman shift peaks as illustrated in Figure 1A without any shift or contaminated peaks with a very strong sharp peak at 300 cm^{-1}. However, Raman spectra of amorphous AgNPs showed characteristic peaks at 52.1 and 146.5 of vibration AgNPs as illustrated in Figure 2B.

3.1.2 | Microscopic class

2D and 3D AFM images and data showed that colloidal SeNPs nanoparticles samples have excellent homogenous surface topography.

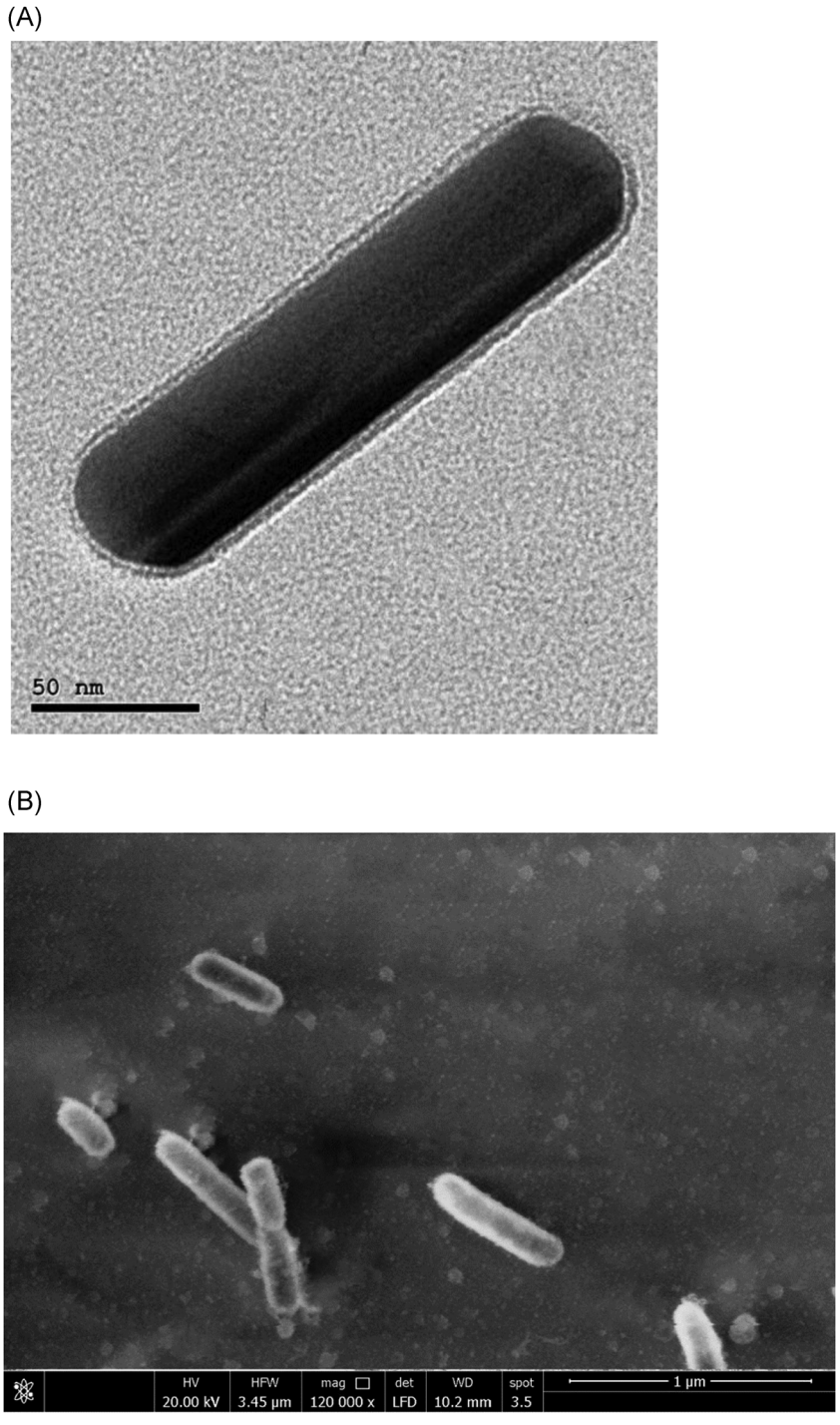

FIGURE 5 (A) Transmission electron microscopy (TEM) image illustrates the colloidal selenium nanoparticles (SeNPs) nanoparticles have rode core-shell nanostructure with a very sharp edge of both core and shell with width size about 30 nm and length about 200 nm and (B) scanning electron microscopy (SEM) image illustrates the rode core-shell nanostructure of SeNPs

In addition, AFM images illustrated the rod shape (blue) with excellent caping of citrate (green) composed core-shell nanostructure with dramatic shape and structure change where most of the literature synthesis spherical SeNPs and the cap was not recognized as shown in Figure 3. Although for AgNPs as shown in Figure 4, AFM images showed its spherical shape with very sharp edges and homogenous in size and shape. SEM and TEM results for AgNPs were found in accordance with AFM results as shown in Figure 6. Colloidal SeNPs nanoparticles have rod core-shell nanostructure with a very sharp edge of both core and shell with width size about 30 nm and length about 200 nm. However, AgNPs have a spherical shape with a size range from 15 to 25 nm. SEM image also determined the rod core-shell nanostructure of SeNPs and spherical shape of AgNPs as shown in Figure 5.

3.1.3 | Index class

BET surface area measured for SeNPs and AgNPs was 25.8 and 70.1 m^2/g, respectively. The nitrogen adsorption-desorption isotherm curve shows unity IV type isotherms with mesopores as shown in Figure 7 for SeNPs and IV type for AgNPs as shown in Figure 8. Zeta sizing and potential illustrated in Table 1 and Figures 7B and 8B, the results showed the very strong stability of SeNPs and AgNPs in aqueous solution due to its high zeta potential value which confirms the colloidal properties of both of them. The DLS curve for SeNPs illustrated the presence of two sharp peaks at sizes about 50 and 200 nm which confirm the presence of two sizes; one for length and the other for the width of rod core-shell nanostructure as shown in Figure 7C. However, the AgNPs curve showed one sharp peak at 15 nm as shown in Figure 8C).

3.2 | Interpretations of AgNPs

3.2.1 | AgNPs improved liver function tests

In the group treated with Ags (0–100 nm), the ALT level was ranged from (31:44 U/L) with the mean equal to (37.5 U/L ± 2.5) showing a

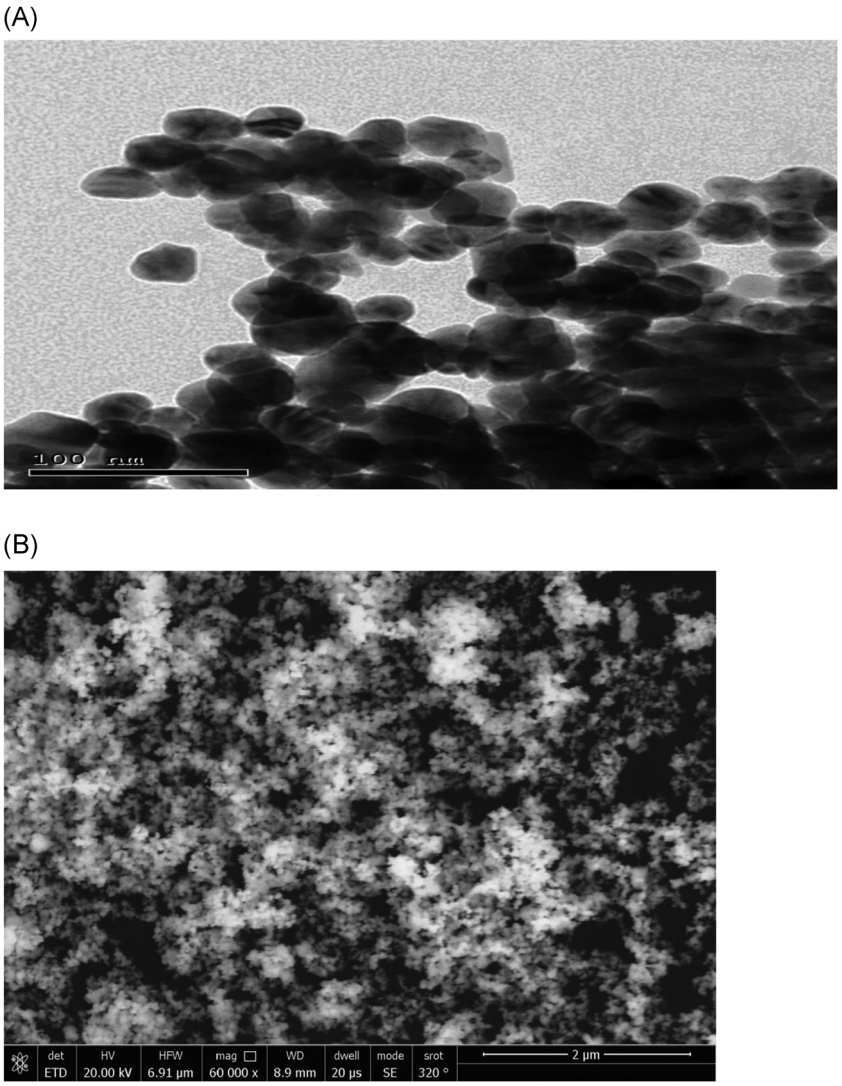

FIGURE 6 (A) Transmission electron microscopy (TEM) and (B) scanning electron microscopy (SEM) images of silver nanoparticles (AgNPs) illustrates the spherical shape of AgNPs with a size range from 15 to 25 nm

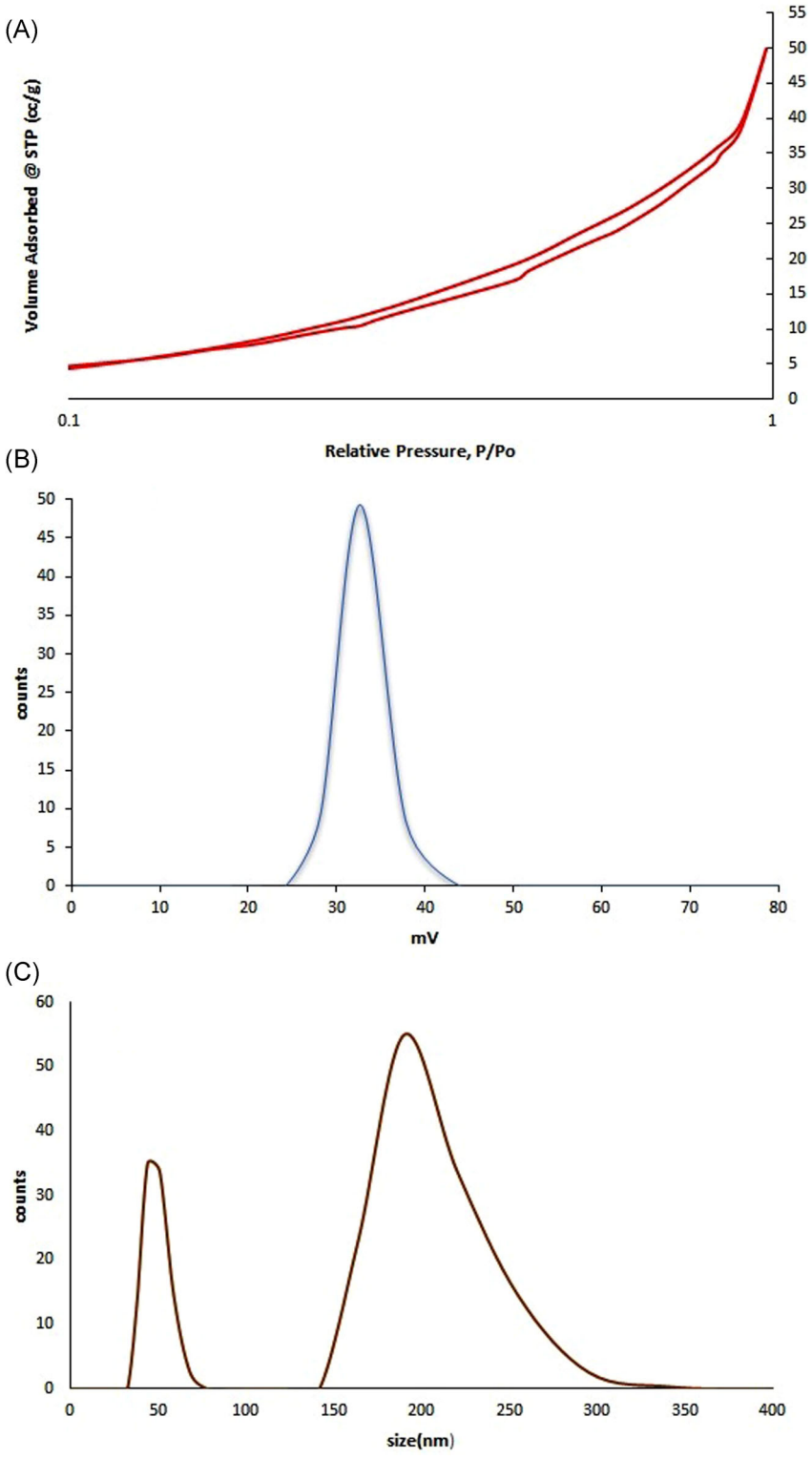

FIGURE 7 (A) The nitrogen adsorption-desorption isotherm curve shows unity IV type isotherms with mesopore selenium nanoparticles (SeNPs). (B) Zeta sizing and potential of SeNPs showed the very strong stability of SeNPs in aqueous solution due to its high zeta potential value which confirms the colloidal properties of both of them. (C) The DLS curve for SeNPs illustrated the presence of two sharp peaks at sizes about 50 and 200 nm which confirm the presence of two sizes; one for length and the other for the width of rod core-shell nanostructure

significant increase compared to normal ones but a significant decrease in comparison to LPS groups ($p < 0.05$). Also, in the group of Ag with large particle size, ALT level was ranged from (35:46 U/L) indicating a significant increase in comparison to the normal group but significantly decreased in comparison to the LPS group ($p < 0.05$); while it shows no significant difference in comparison to the group of Ag with small particle size. Similarly, AST level was ranged from (19:22 U/L) with the mean equal to (20.3 U/L ± 0.6) showed a significant decrease in comparison to LPS or NAC groups ($p < 0.05$). In NAC + AgL group, the AST level showed (19.7 U/L ± 0.6) significant increase in comparison to normal while it causes a significant decrease in AST level in comparison to LPS or NAC group ($p < 0.05$) as shown in Figure 9A,B.

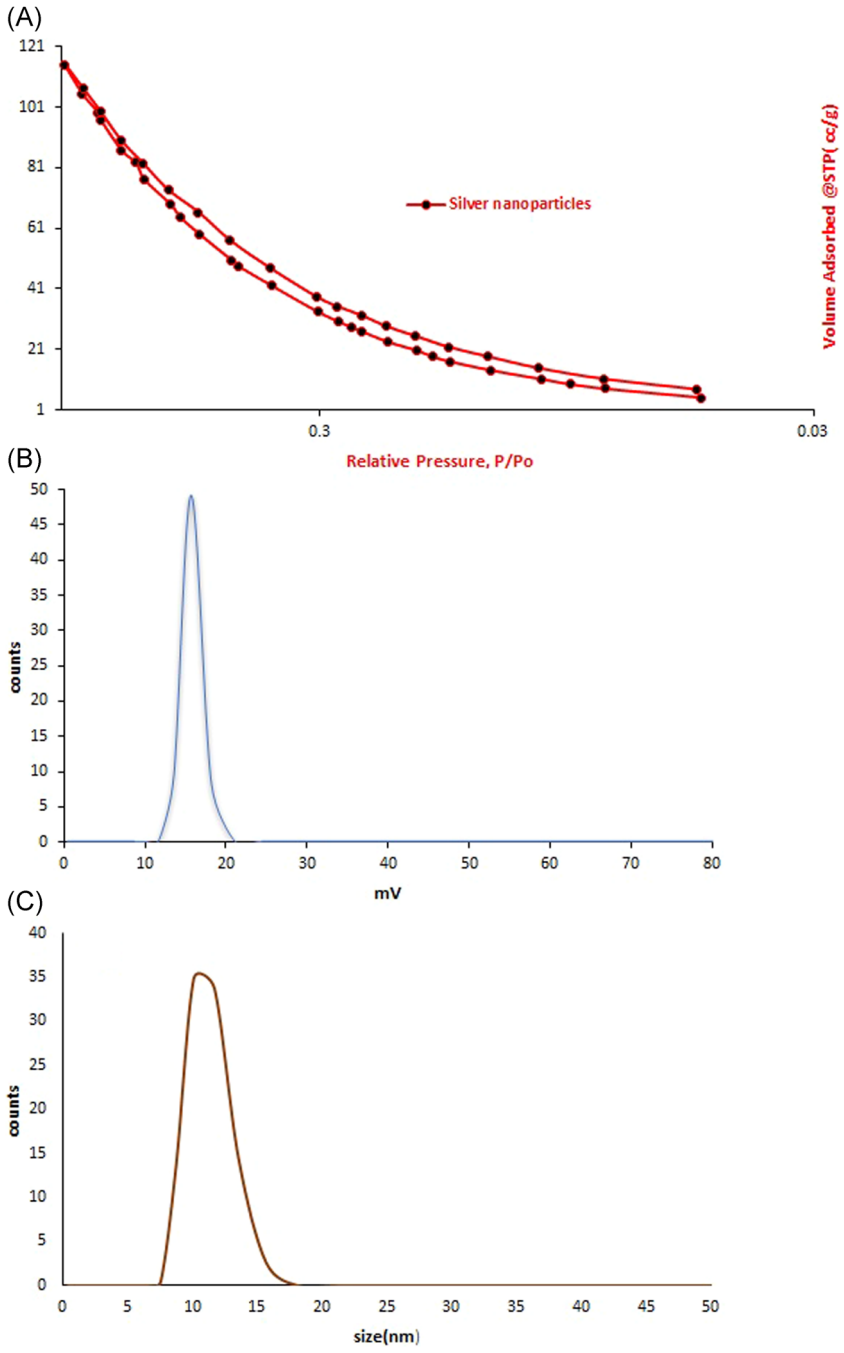

FIGURE 8 (A) The nitrogen adsorption-desorption isotherm curve shows unity IV type isotherms with mesopores of silver nanoparticles (AgNPs). (B) Zeta sizing and potential of AgNPs showed the very strong stability of AgNPs in aqueous solution due to its high zeta potential value which confirms the colloidal properties of both of them. (C) DLS curve of AgNPs showed one sharp peak at 15 nm

TABLE 1 Summary of Zeta size and potential of all silver and selenium nanoparticles (AgNPs and SeNPs) samples

Samples	Size (nm)	potential
SeNPs	45	−32.1
AgNPs	15	−18.9

Note: BET method (the Brunauer–Emmett–Teller isotherm) used to determine the specific surface area by pore and surface area analyzer manufacturer by Quantachrome, model of NOVA touch LX2. Zeta potential is achieved by the zeta potential analyzer.

3.2.2 | Antioxidative and anti-inflammatory effects of AgNPs

The bacterial infection in the LPS group resulted in a 2.6-fold decrease in the lipid peroxidation marker expressed as GSH compared with control liver slices indicating liver damage. Treatment with AgS increased GSH by around 40% and similarly In AgL group, the treatment caused a twofold increase in GSH level compared to LPS group Figure 9C.

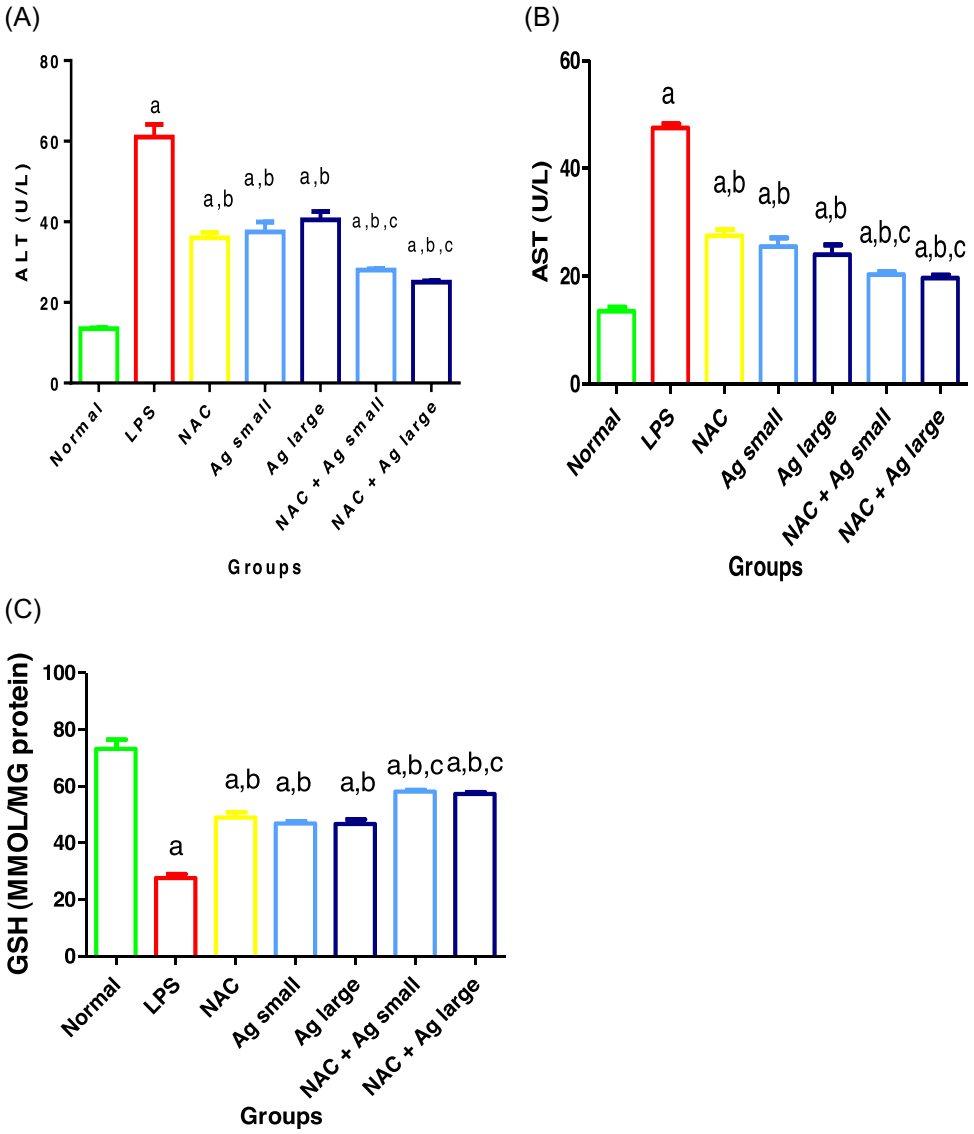

FIGURE 9 (A) Effect of treatment with AgNPs on ALT levels in the studied groups. (B) Effect of treatment with AgNPs on AST levels in the studied groups. (C) Effect of treatment with AgNps on glutathione (GSH) levels in the studied groups. Treatment with both small and large Ag nanoparticles significantly decreased liver function tests in comparison with the LPS group. The bacterial infection in the LPS group resulted in a 2.6-fold decrease in the lipid peroxidation marker expressed as GSH compared with control liver slices indicating liver damage. Each value represents the mean of six experiments ± SD. [a]Significant difference versus the control group; [b]Significant difference versus the LPS group, [c]Significant difference versus the NAC group. ALT, alanine aminotransferase; AST, aspartate aminotransferase; AgNPs; silver nanoparticles; LPS, lipopolysaccharide

The anti-inflammatory properties of AgNPs in Liver slices were assessed by measuring the IL-6 and TNF-α levels. Treatment with both AgS and AgL resulted in the decrease of the anti-inflammatory IL-6 and the decrease of the proinflammatory TNF-α. Upon treatment with AgS, the IL-6 decreased by more than 1.6-fold while AgL decreased it by 1.5-fold. On the other hand, AgS treated group decreased TNF-α by 21% compared to the diseased LPS group while AgL surpassed this to reach 32% decrease in the levels of TNF-α as shown in Figure 10.

3.2.3 | Histopathological and immunohistochemistry assessment

H&E staining revealed significant changes obtained in the histological examination between the control, LPS, and treated groups with small and large particles of AgNPs. In the LPS group, the liver tissue shows activation of Kupffer cells and sporadic hepatocytes necrosis while both the AgS and the AgL groups showed slight activation of Kupffer cells and few necrosis

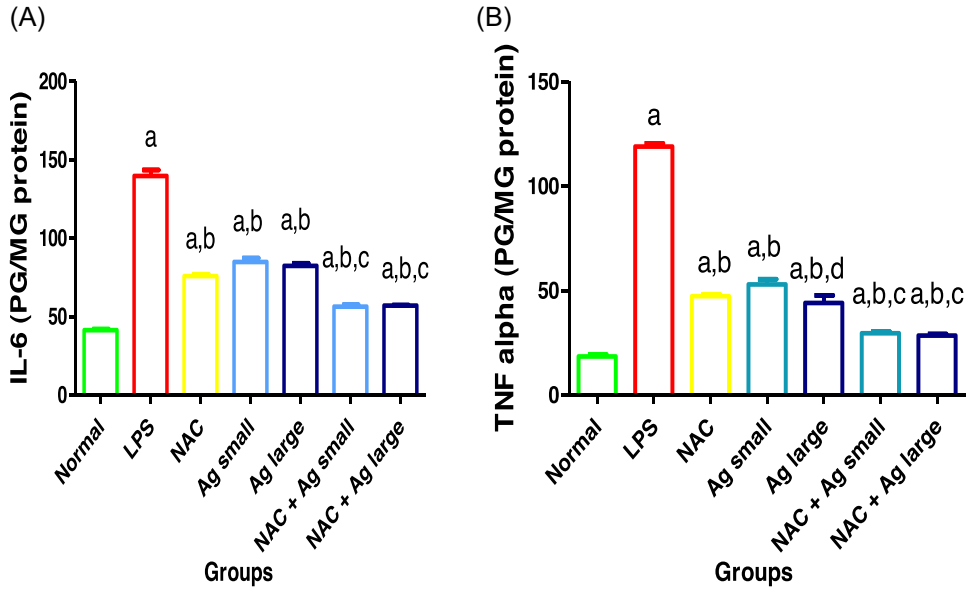

FIGURE 10 (A) Effect of treatment with AgNPs on the IL-6 levels in the studied groups. (B) Effect of treatment with AgNPs on the TNF-α levels in the studied groups. Treatment with both AgS and AgL resulted in the decrease of the anti-inflammatory IL-6 and the decrease of the proinflammatory TNF-α. Each value represents the mean of six experiments ± SD. [a]Significant difference versus the control group; [b]significant difference versus the LPS group, [c]Significant difference versus the NAC group; [d]Significance in relation to AgS. AgNPs, silver nanoparticles; IL-6, interleukin-6; LPS, lipopolysaccharide; TNF-α, tumor necrosis factor-α

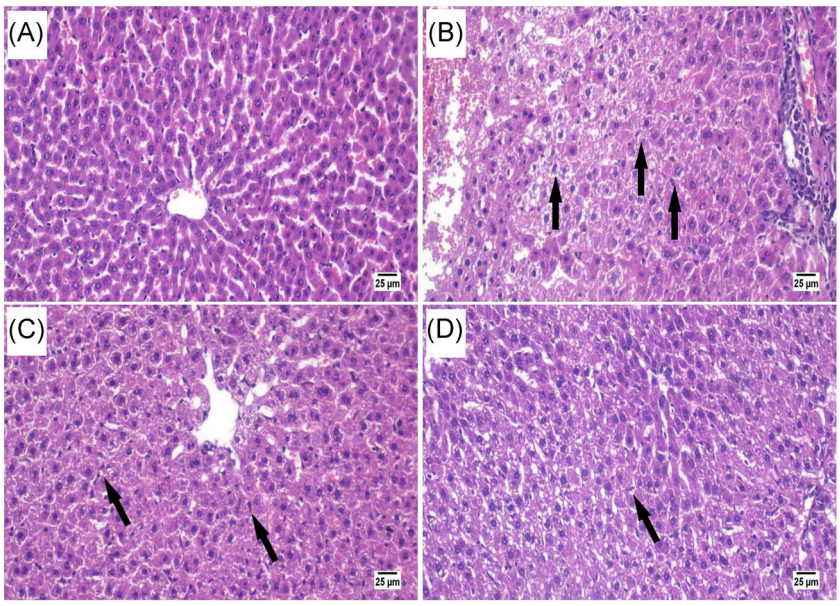

FIGURE 11 H&E stain (×400). (A) Liver slices of the control group showed no histopathological changes. (B) Liver of LPS group showing Kupffer cells activation and necrosis of sporadic hepatocytes. (C) Liver slices treated with AgS showed some Kupffer cells activation and little necrosis of sporadic hepatocytes. (D) Liver slices treated with AgL showed slightly Kupffer cells' activation and little necrosis of sporadic hepatocytes. H&E, hematoxylin and eosin; LPS, lipopolysaccharide

effects of hepatocytes (Figure 11). Immune expression of CD68 in liver slices is illustrated in Figure 12 The liver slices of the control group showed normal expression of CD68 cells. On contrary, CD68 expression was significantly increased in the LPS group compared to the control group. However, the AgS and the AgL treated groups exhibited a significant improvement in the reduction of CD68 expression in comparison to the LPS group.

3.3 | Interpretations of SeNPs

3.3.1 | SeNPs improved liver function tests and reduced oxidative stress marker

After treatment of HBV-hepG2 cell lines with SeNPs, both ALT (U/L) and AST (U/L) levels were increased by 1.7 and 2.5-folds while the MDA concentration decreased. SeNPs administration enhanced the

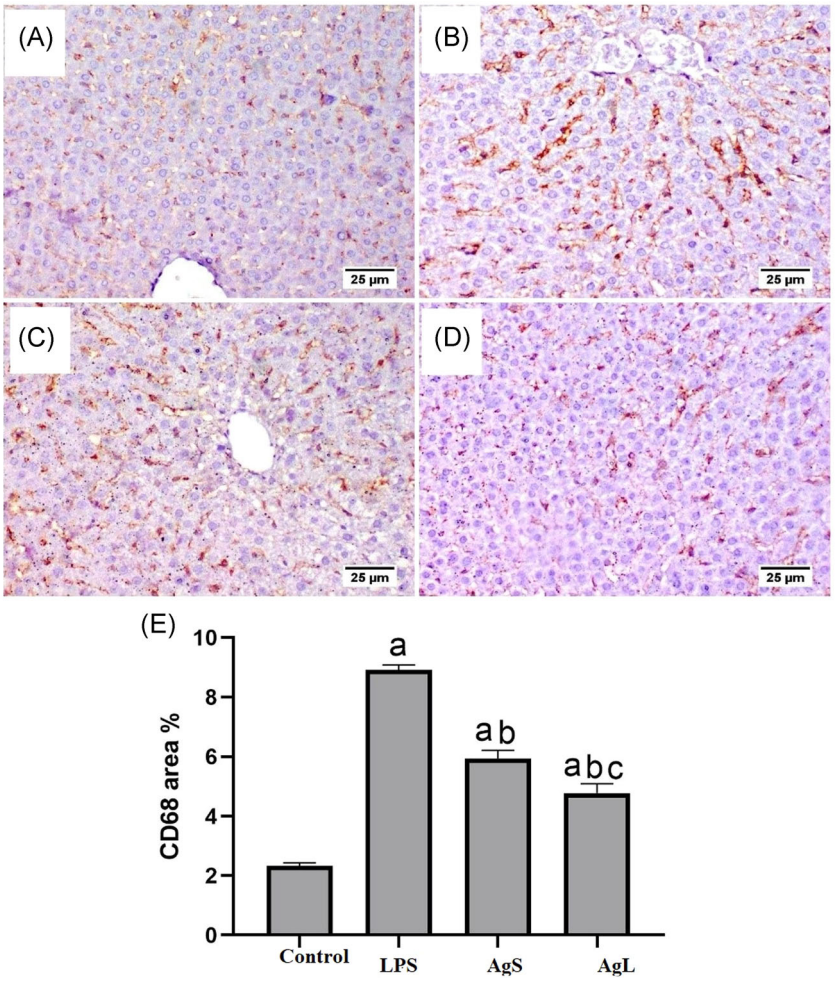

FIGURE 12 Immunostaining of CD68 in liver tissue. (A) Liver slices of the control group showed normal expression of CD68 cells. (B) Liver of LPS group showing a significant increase in CD68 expression. (C) Liver slices treated with AgS showed a significant improvement in reduction of CD68 expression and (D) Liver slices treated with AgL showed a greater reduction of CD68 expression compared with other groups. (E) Quantification of CD68 positive cells as area % of expression. Value presented as means ± SE significant difference was considered at $p < 0.05$. [a]significant difference versus the control group; [b]significant difference versus the LPS group, [c]significant difference versus the AgS treated group. LPS, lipopolysaccharide

TABLE 2 Effect of treatment with SeNPs on liver function enzymes and MDA in the control, HBV, and HBV-NP groups

Group	ALT (U/L)	AST (U/L)	MDA (g/dl)
Control	37.59 ± 3.56	38.42 ± 3.59	1.03 ± 0.18
HBV cell line HepG2 (HBV)	75.38[a] ± 5.28	85.1[a] ± 16.12	1.4[a] ± 0.24
HBV cell line HepG2 treated with SeNPs (HBV-NP)	53.8[a] ± 3.89	57.11[a] ± 4.49	1.2[a] ± 0.28

Note: Statistical analysis was performed using one-way ANOVA followed by Tukey's multiple comparison post hoc test.

Abbreviations: ANOVA, analysis of variance; ALT, alanine aminotransferase; AST, aspartate aminotransferase; MDA, malondialdehyde.

[a]Significant difference versus the control group.

liver function tests and decreased the level of both enzymes as well as decreased the secretion of MDA by 1.2-fold (Table 2).

3.3.2 | Anti-inflammatory effects of SeNPs in HBV-replicating human HCC cell line HepG2

SeNPs showed 1.3-fold and 1.5 decreases in both proinflammatory markers TNF-α and TGF levels in HepG2 cell lines after administering of SeNPs. These values were decreased significantly after treatment. Additionally, SeNPs decreased the level of IL-8 by 46% and IL-2 by 43%. Treatment with SeNPs lowered the level of all proinflammatory markers significantly compared to the control group (Figure 13).

3.3.3 | Effects of SeNPs on DNA fragmentation

The effect of the administration of SeNPs on DNA fragmentation in HepG2 cell lines is illustrated in Figure 14. A significant more than 8-fold increase in the tail length and a 3.7-fold increase in tail DNA%

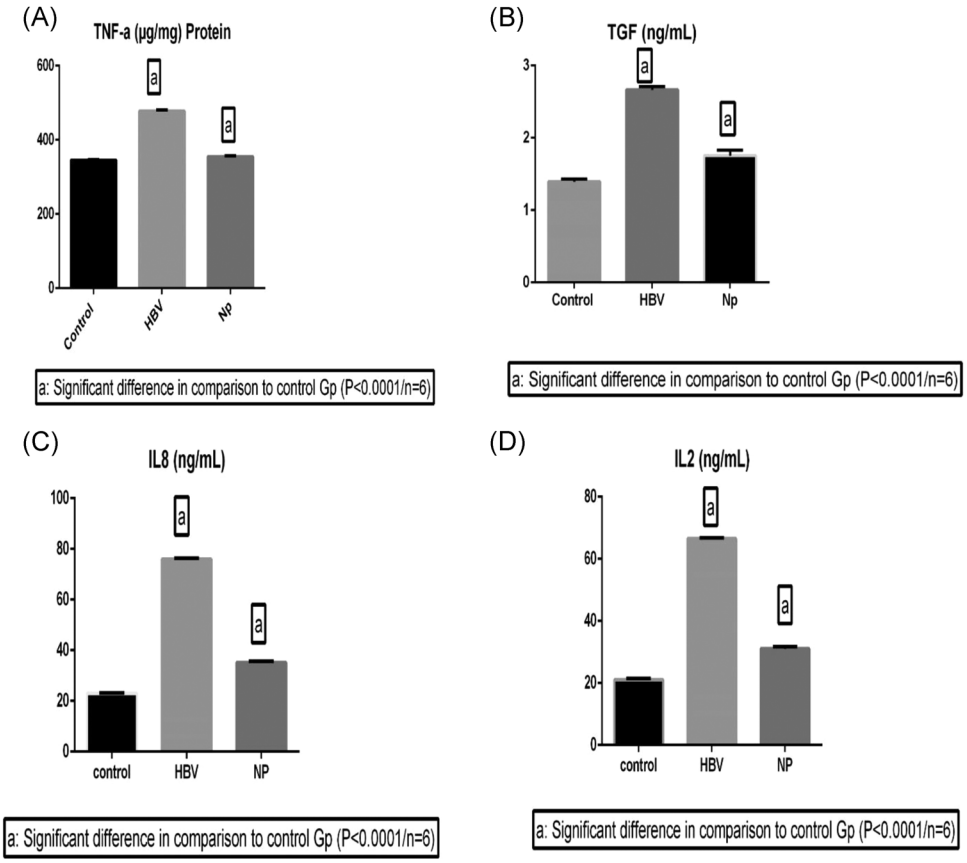

FIGURE 13 (A) Effect of treatment with SeNPs on the TNF-α levels in the control, HepG2 cell lines, and SeNPs treated groups. (B) Effect of treatment with SeNPs on the TGF levels in the control, HepG2 cell lines, and SeNPs treated groups. SeNPs showed 1.3-fold and 1.5 decreases in both proinflammatory markers TNF-α and TGF levels in HepG2 cell lines after administering of SeNPs. (C) Effect of treatment with SeNPs on the IL-8 levels in the control, HepG2 cell lines, and SeNPs treated groups. (D) Effect of treatment with SeNPs on the IL-2 levels in the control, HepG2 cell lines, and SeNPs treated groups. Additionally, SeNPs decreased the level of IL-8 by 46% and IL-2 by 43%. Each value represents the mean of six experiments ± SD. [a]Significant difference versus the control group. IL-8, interleukin-8; SeNPs, selenium nanoparticles; TGF, tumor growth factor; TNF-α, tumor necrosis factor-α

(tDNA%) was shown in the HepG2 cell lines infected with HBV. Treatment with SeNPs significantly protected HepG2 cell lines from DNA damage as indicated by a decrease in the tDNA% by 17% compared to the diseased group.

4 | DISCUSSION

Recently, studies focused on the ability of nanoparticles in drug delivery and targeting, leading to the treatment of various liver diseases.[13,14] Consequently, this study investigated the effects of both AgNPs and SeNPs on liver tissue injury due to viral and bacterial causes. The study showed different mechanisms for the effect of AgNPs on liver tissue even at low concentrations; either through the particle size of the AgNPs or through the downregulation of secretion of cytokines by hepatic cells, which may lead to HSC activation.

Other evidence was observed in the histological changes including, necrosis and hepatocellular degeneration that were dose-dependent. Several studies confirmed that the liver is the main target organ for the effect of AgNPs and showed that liver tissue after treatment with AgNPs exposure may be associated with reduction of oxidative stress.[14,15] It is known that oxidative stress is the main mechanism by which AgNPs affect the treatment of injured liver tissues.[16,17] In this study, markers of oxidative stress and inflammatory mediators were measured in the liver tissues. We observed a significant decrease in GSH level and a significant increase in TNF-α and IL-6 in hepatocytes. Our study suggests that the ability of AgNPs to cause a significant decline in the inflammatory markers leads to reduce apoptosis through inflammatory and oxidative stress mechanisms.

Several previous studies have focused on the effect of nanoparticle size on cytotoxicity and cellular uptake.[18] In this study, AgNPs of two different sizes classified as small particle size (10 and 75 nm) and large particle size (250–300 nm) at different concentrations were included in the treatment of bacterially infected liver slices together with NAC. Activation of HSCs is significant in the development of liver disease through the secretion of many cytokines. The results of the Elisa assay demonstrated that the anti-inflammatory effects exerted by AgNPs on HSCs are size- and dose-dependent.

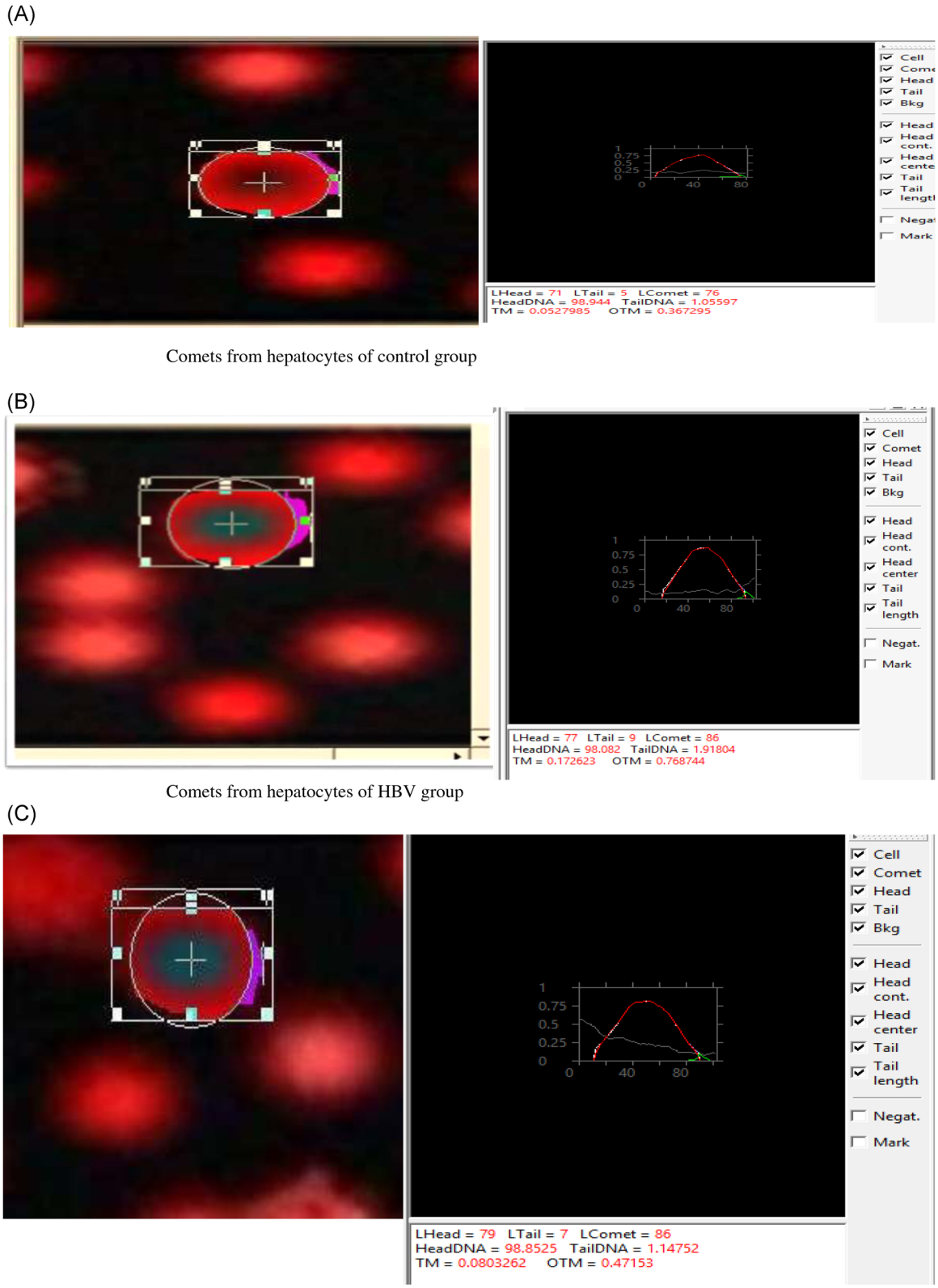

FIGURE 14 Effect of treatment with SeNPs on DNA fragmentation. Comets from hepatocytes: (A) control, (B) HBV, (C) SeNPs treated. Treatment with SeNPs significantly protected HepG2 cell lines from DNA damage as indicated by a decrease in the tDNA% by 17% compared to the HBV group. HBV, hepatitis B virus; SeNPs, selenium nanoparticles

Larger AgNPs showed a significant reduction in TNF-α than the smaller particles, while for the anti-inflammatory marker; IL-6, both small and large particles showed a significant reduction in IL-6 compared to the LPS group. According to our study, the other mechanism by which AgNPs can treat the liver bacterial infection occurs through its effects on the upregulation of antioxidants (GSH) and this was clearly obvious in the groups treated with small and large AgNPs compared to the LPS group.

Moreover, AgNPs affected successfully the liver function tests, this was confirmed by the significant decrease of AST and ALT levels in groups treated with NAC together with small and large particles compared with the LPS group and group treated with NAC only, which indicate a significant protective role of AgNPs. Therefore, the reducing effects of AgNPs on production of important cytokines as well as liver function tests which were also confirmed by other previous studies may suppress the progression of hepatic fibrosis; however, the detailed mechanisms require more studies.[19] The size of AgNPs is highly significant in the cellular uptake by tissues, and thus affecting their bioactivity.[20] The design of nanoparticles for medical applications should take into consideration the particle size to obtain the maximum effect.

There are several causes for chronic liver disease including; alcohol addiction, fatty liver, fibrosis, hepatitis B and C, and cirrhosis.[21] Recently SeNPs are considered a potential tool for treatment of cancers due to their chemical protective agent against toxic side effects of anticancer drugs.[22] In the present study, the treatment of HBV-replicating human cell line HepG2 with SeNPs showed significant alterations in inflammatory mediators produced by injured liver tissue and DNA fragmentation.

Endocytosis has been proved as an important cellular uptake mechanism for nanoparticles. Many previous studies confirmed that SeNPs divide into smaller particles under the acidic conditions of the lysosomes, which helps the metabolism of SeNPs and the release of the loaded drugs.[23]

Lipid peroxidation markers are products of the oxidation and reduction process, including highly toxic compounds.[24] These markers are considered to be a significant factor in cancer prevalence and recurrence. In addition, many studies have shown that alterations in lipid oxidation and inflammatory markers level in cells affect cell apoptosis and in turn, could be used in treatment.[25]

Our results agree with another study conducted by Wang et al.[26] who suggested that this injury is caused due to increase in the oxidative stress process in the liver, and this was clearly obvious in our study which showed a significant reduction in MDA levels in the treated group with SeNPs compared to HepG2 cell lines. Moreover, our results were also confirmed by a recent study[23] which found that HBV causes inflammation and chronic liver injury which affects the damage of DNA, our current findings showed a significant decrease in the inflammatory markers; TNF-α, TGF, IL-6, and IL-2 in the HepG2 cell lines treated with SeNPs compared to HBV-HepG2 cell lines. Additionally, the increase in DNA damage in HBV cell lines may be due to the release of free radicals including nitric oxide reactive species (NOS) and reactive oxygen species (ROS) which leads to liver injury.[27] These ROS led to inflammatory responses, necrosis of liver cells, and fibrogenesis.[28]

Our current results of comet assay showed that the treatment of HBV-cell lines with SeNPs caused a significant decrease in DNA damage compared to HBV-cell lines, these results were reported also by another study.[29] Taken into consideration, previous studies have shown that SeNPs has a significant therapeutic action for several diseases such as inflammation, cancer, and viral infection,[30,31,32] for this reason, this nanosystem is drawing great attention in the field of therapy due to its higher stability, antiviral activity, anti-inflammatory activity, and low toxicity compared to other nanoparticles.

5 | CONCLUSION

In view of the present study, the efficacy of AgNPs was investigated by different biochemical approaches and it was particle dose and particle-dependent. The biochemical alterations in the inflammatory and oxidative stress markers may be an indication of the antioxidant activity and the inhibitory activity of proliferation of injured cells caused by AgNPs in liver tissue. On the other hand, SeNPs played a potential role in reducing DNA damage as well as reduction of several cytokines in HBV-cell lines showing its greater effect as anti-inflammatory and antiviral nanoparticle in comparison with AgNPs. Taken together, both nanoparticles might be an innovative approach for treatment of viral and bacterial liver infection, however, more studies are needed to support the use of AgNPs and SeNPs for human disease treatment and prevention.

CONFLICT OF INTERESTS

The authors declare that there are no conflicts of interest.

ETHICS STATEMENT

The study protocol was approved by the Ethics Committee of the Faculty of Pharmacy, MSA University, Ethics Committee (**code: PH8/EC8/2019F).2019F)**. I understand that all information I provide for this study will be treated confidentially. The signed Consent ensures that the Publisher has the Author's permission to publish the relevant Contribution.

AUTHOR CONTRIBUTIONS

Sameh S. Gad and Sameh H. Ismail participated in the study design, practical work especially molecular biology as well as interpretation of data and manuscript preparation. Sherine M. Ibrahim and Dina S. Abdelrahim participated in practical work, interpretation of data, and manuscript preparation. All authors read and approved the manuscript and all data were generated in-house and that no paper mill was used.

DATA AVAILABILITY STATEMENT

All data generated or analyzed during this study are included in this published article.

ORCID

Sherine M. Ibrahim http://orcid.org/0000-0002-2755-1641

REFERENCES

[1] R. Shanmuganathan, D. MubarakAli, D. Prabakar, H. Muthukumar, N. Thajuddin, S.S. Kumar, A. Pugazhendhi, *Environ. Sci. Pollut. Res.* **2018**, *25*(11), 10362.
[2] J. Rane, R. Jadhao, R. Bakal, *J. Innov. Pharm. Biol. Sci.* **2016**, *3*(2), 24.
[3] M. Saravanan, S.K. Barik, D. MubarakAli, P. Prakash, A. Pugazhendhi, *Microb. Pathog.* **2018**, *116*, 221.
[4] A. Pugazhendhi, T.N.J.I. Edison, I. Karuppusamy, B. Kathirvel, *Int. J. Pharm.* **2018**, *539*(1), 104.
[5] Y. Huang, Y. Luo, J. Zheng, T. Chen, *ACS Appl. Mater. Interfaces* **2014**, *6*, 19217.
[6] B. Zhou, Y. Huang, F. Yang, W. Zheng, T. Chen, *Chem.–Asian J.* **2016**, *11*, 1008.
[7] T. Liu, L. Zeng, W. Jiang, Y. Fu, W. Zheng, T. Chen, *Nanomedicine* **2015**, *11*, 947.
[8] X.-F. Zhang, Z.-G. Liu, W. Shen, S. Gurunathan, *Int. J. Mol. Sci.* **2016**, *17*(9), 1534.
[9] M.A. Akram, M. Tembhre, R. Jabeen, S. Khalid, M.A. Sheikh1, A. Jan, U. Farooq, M. Amin, *J. King Saud. Univ. Sci.* **2019**, *43*, 50.
[10] K.S. Suvarna, C.B.J. Layton, *Bancroft's theory and practice of histological techniques*, 8th ed. **2018**.
[11] S. Ismail, G. Mohamed, A. Amer, M. Amer, *Nano Biomed. Eng.* **2020**, *12*(4), 338.
[12] A. Reitznerová, M. Šuleková, J. Nagy, S. Marcinčák, B. Semjon, M. Cert, T. Klempová, *Molecules* **2017**, *49*(12), 3367.
[13] P. Suchithra, G. Reju, J. Myeong, Y. Yong, *Int. J. Nanomedicine.* **2017**, *12*, 6997.
[14] H. Ebaid, M. Habila, I. Hassan, J. Al-Tamimi, M.S. Omar, A. Rady, I.M. Alhazza, *Comb. Chem. High Throughput Screen.* **2020**, *11*(3040).
[15] E. Barcińska, J. Wierzbicka, A. Zauszkiewicz-Pawlak, D. Jacewicz, A. Dabrowska, I. Inkielewicz-Stepniak, *Oxidative Med. Cell. Longev.* **2018**, *2018*, 8251961.
[16] C. Bacchetta, A. Ale, M.F. Simoniello, S. Gervasio, C. Davico, A.S. Rossi, M.F. Desimone, G. Poletta, G. López, J.M. Monserrat, J. Cazenave, *Ecol. Indic.* **2017**, *76*, 230.
[17] I. Pinzaru, D. Coricovac, C. Dehelean, E.A. Moacă, M. Mioc, F. Baderca, I. Sizemore, S. Brittle, D. Marti, C.D. Calina, A.M. Tsatsakis, C. Şoica, *Food Chem. Toxicol.* **2018**, *111*, 546.
[18] D. McShan, P.C. Ray, H. Yu, *J. Food Drug Anal.* **2014**, *22*, 116.
[19] T. Wu, M. Tang, *J. Appl. Toxicol.* **2018**, *38*, 25.
[20] M.A. Abdelhalim, B.M. Jarrar, *Lipids. Health Dis.* **2015**, *10*, 1662011.
[21] J. Ebaid Al-Tamimi, M.A. Habila, I. Hassan, A.M. Rady, I.M. Alhazza, *J. King Saud Univ. Scien.* **2021**, *33*, 101356.
[22] X. Jia, Q. Liu, S. Zou, X. Xu, L. Zhang, *Carbohydr. Polym.* **2015**, *117*, 434.
[23] E. Karavelioglu, M.G. Boyaci, N. Simsek, M.A. Sonmez, R. Koc, M. Karademir, M. Guven, O. Eser, *Acta Cirúrgica Brasileira* **2015**, *30*(6), 394.
[24] H. Steinbrenner, S. Al-Quraishy, M.A. Dkhil, F. Wunderlich, H. Sies, *Adv. Nutr.* **2015**, *6*, 73.
[25] B. Zhou, Y. Huang, F. Yang, W. Zheng, T. Chen, *Chem.–Asian J.* **2016**, *11*, 1008.
[26] N. Wang, H.Y. Tan, S. Li, Y. Xu, W. Guo, Y. Feng, *Oxidative Med. Cell. Longev.* **2017**, *2017*, 1.
[27] K.A. Amin, S. khalid, T. Fawziah, *Biol. Trace Elem. Res.* **2017**, *175*(1), 136.
[28] M. Lesnichaya, E. Karpova, B. Sukhov, *Cell. Colloids Surf. B Biointerfaces* **2021**, *197*, 111381.
[29] K. Bai, M. Parola, *Nutrients* **2020**, *12*(3), 857.
[30] A.H. Abd El-Rahim, O.M. Abd-Elmoneim, N.A. Hafiz, *Jordan J. Biol. Sci.* **2017**, *10*, 159.
[31] J. Feng, C. Guo, Y. Zhu, L. Pang, Z. Yang, Y. Zou, X. Zheng, *Int. J. Clin. Exp. Med.* **2014**, *7*, 4063.
[32] I. Hassan, H. Ebaid, J. Al-Tamimi, M.A. Habila, I.M. Alhazza, A.M. Rady, *J. King Saud Univ. Sci.* **2021**, *33*, 101265.

How to cite this article: S.S. Gad, D.S. Abdelrahim, S.H. Ismail, S.M. Ibrahim, *J. Biochem. Mol. Toxicol.* **2021**, e22972. https://doi.org/10.1002/jbt.22972